Acta Polytechnica **65**(3):288–295, 2025
https://doi.org/10.14311/AP.2025.65.0288

Published by the Czech Technical University in Prague

VORTICES IN THE WAKE PAST ADJUSTABLE CAR SPOILER IN OPEN AND CLOSED CONFIGURATION STUDIED EXPERIMENTALLY BY PIV

Vojtěch Janský[a,*], Zdeněk Hejda[b], Daniel Duda[a], Vitalii Yanovych[a,c], Václav Uruba[a,d]

[a] *University of West Bohemia in Pilsen, Faculty of Mechanical Engineering, Univerzitní 22, 306 14 Pilsen, Czech Republic*

[b] *Škoda Auto University, Department of Machinery and Electrotechnics, 160 00 Prague, Czech Republic*

[c] *Research and Testing Institute Pilsen, Tylova 46, 301 00 Pilsen, Czech Republic*

[d] *Czech Academy of Sciences, Institute of Thermomechanics, Dolejškova 15, 180 00 Prague, Czech Republic*

[*] corresponding author: vjansky@fst.zcu.cz

Abstract. A complex adjustable car spoiler opens or closes in dependence on ride properties: the closed state increases negative lift (better for curves), while the open state ensures lower drag (better for straight segments of the road). Both these configurations are studied by using Particle Image Velocimetry method in a wind tunnel at model scale. The three measured planes are perpendicular to the main flow. The wake is characterised by upwind (stronger past the closed variant) and by a pair of wing-tip vortices, although the spoiler wing has no end, it is rounded downwards instead. These vortices are stronger past the closed variant, they migrate towards each other, while their positions correlate by about 30 %. The circulations of both vortices are strongly correlated by about 90 % for the closed case, while this correlations is much smaller (~ 25 %) for the open case.

Keywords: Car, spoiler, wind tunnel, particle image velocimetry, wake, vortex.

1. Introduction

In the car industry, spoiler is established and well known part coming from the car racing branch. As the racing car has become faster over time, the need to keep them capable of steering through bends at higher speeds without loosing the car control. The most dangerous situation, where the driver loses control, is the absence of grip between tires and the surface of the track. The gripping force correlates with the track and tire's surface material and the resulting force reaction perpendicular to the contact surface that pushes the tire and track together. The designers developed a solution to this problem in a form of a car part named *spoiler*, which may be seen as flipped airplane wing, increasing the pressure force (negative lift) while not significantly increasing the weight of the car, and ideally without increasing the car's aerodynamic drag. Through the history, the design of the spoiler developed and not only fixed spoilers are used but also *retractable* or *adjustable spoilers*.

An additional function is required from spoilers used for trucks. Improvements are required to the aerodynamics and to reduction of a vortex coming from the airflow against the trailer behind the truck. These might be optimised also for the configuration without the trailer.

Negative lift coming from the spoiler geometry is quadratically dependent on the car speed [1]. However, optimisation of fixed spoiler design for negative lift is for specific speed range – air velocity. An adjustable spoiler might help to wider the optimal speed range of the car and improve its performance on straight or curved roads.

Vortices, that are created by air while passing the spoiler have a strong effect on the aerodynamic [2]. Such vortex is a long-lived structure, whose effect does not limit to the car with a spoiler, but it affects the aerodynamics of cars behind [3–5]. Understanding their behaviour is an important precursor of an optimised design. Therefore, we decided to study this behaviour in our research.

2. Materials and methods

2.1. Model

The basic idea of the investigated spoiler comes from professor Zdeněk Hejda from the Škoda Auto University. Unfortunately, prof. Hejda has discontinued his research. Therefore, we do not know the ideas and motivations behind his design. This complex-shaped spoiler has two prismatic airfoils in its active part. The second one can be adjusted during the ride to two positions:

(1.) The *open* configuration, where the second airfoil is horizontal and there is a gap between the trailing edge of the first airfoil and leading edge of the second one.

(2.) The *closed* configuration, where the second airfoil almost touches the first one (see Figure 1 for easier imagination).

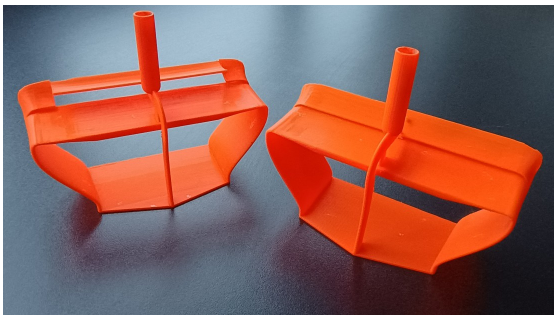

(A). Photograph of both models: open left, closed right.

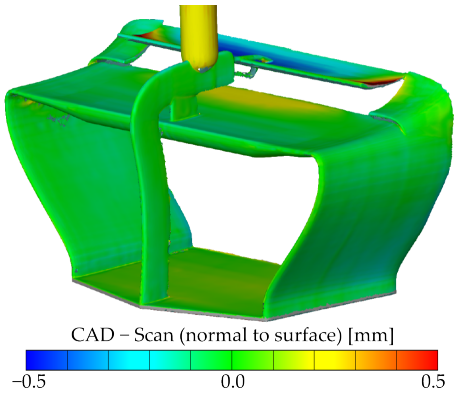

(B). Differences between optical scan of the model and CAD.

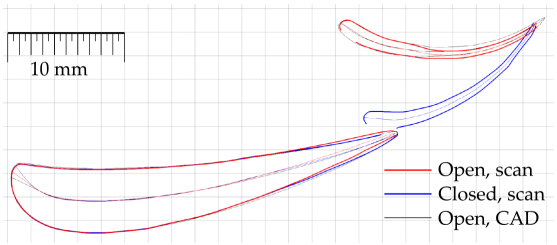

(C). Airfoil profiles of the prismatic part of the spoiler.

FIGURE 1. Top: photograph of the models used for the measurement made of Polymerized lactic acid (PLA). Middle: real geometry obtained by using optical scanning by `Atos Core` device compared with original design (CAD – computer-aided design) made by prof. Zdeněk Hejda. Bottom: xy-section of the geometry focused on the airfoil profile in the prismatic part; single grey square represents $2 \times 2\,\mathrm{mm}^2$.

The model is 3D printed using polymerised lactic acid (PLA) [6] in two variants – first one is the open variant of the adjustable spoiler and second one is the closed state. It was impossible to scale the adjusting mechanism to the size suitable for wind tunnel experiments. Photograph of both models is shown in Figure 1a. Both printed models are scanned using optical 3D scanner `Atos Core` from the company `Gom` [7]. The neon-orange color is found to be very suitable as the fluorescent effect is activated by the blue light used for 3D scanning [8–10], but it is inactive in green light used for PIV measurement. Therefore, the object is well visible by the scanner without any need for some extra layer of coating [10]. And, at the same time, it is

Dimension	Open [mm]	Closed [mm]	CAD [mm]
1st airfoil chord	33.2	33.2	33.3
2nd airfoil chord	16.9	16.7	17.7
1st airfoil thickness	5.41	5.38	5.49
2nd airfoil thickness	1.37	1.42	1.40
2nd leading edge thick.	1.16	1.18	1.25
Dist. of leading edges	8.04		×

TABLE 1. Dimensions of the airfoil profiles.

effectively black if it is illuminated by green light and observed through green filter during a PIV measurement. Figures 1b, 1c and Table 1 show the comparison of optical scan and original CAD developed by prof. Hejda. When the spoiler opens, the second airfoil rotates around its trailing edge into almost horizontal position. The distance between the leading edges in open and closed configurations is 8 mm.

2.2. Wind tunnel

The experiment is carried out in a wind tunnel [11] at the University of West Bohemia in Pilsen. This open low-speed wind tunnel is powered by a radial fan, its working fluid is ambient air and the velocity in test section is stabilised via back-loop of pressure drop at the contraction section. The test section cross-section has dimensions of $300 \times 200\,\mathrm{mm}^2$. The tested model is placed in various distances upwind from the measured plane: 88, 180, and 273 mm, see Figure 2. Therefore, the boundary layer thickness is different at each location, but this effect is considered to be only small and to not affect the effective wind velocity at the model position. Reference velocity U_{ref} measured via the pressure drop along the wind tunnel contraction section was $5\,\mathrm{m\,s}^{-1}$.

2.3. Measurement method

Particle Image Velocimetry (PIV) in stereo configuration [12–14] is used to measure the velocity fields around the model in discussed locations. The principle of this method is that there are small particles carried by the fluid – in current setup droplets of glycerin-based solution known under commercial name Safex. These particle are small enough to neglect the inertial and gravitational forces, which scale with particle volume, i.e. as $\sim r^3$, while the forces from fluid-particle interaction scale as $\sim r^2$ or even as $\sim r^1$ in the case of laminar flow at low relative velocities. Therefore, the volumetric forces are much smaller than forces from the fluid and it can be assumed, that these particles follow the motion of the fluid. The experience confirms the usage of this technique up to very high velocities, see e.g. the work of Koschatzky et al. [15] or measuring inside of a model steam turbine [16, 17] or even in supersonic flows [18]. Hong et al. [19] even used natural snow as tracer particles for PIV method. The particles carried by the fluid are illuminated in a plane

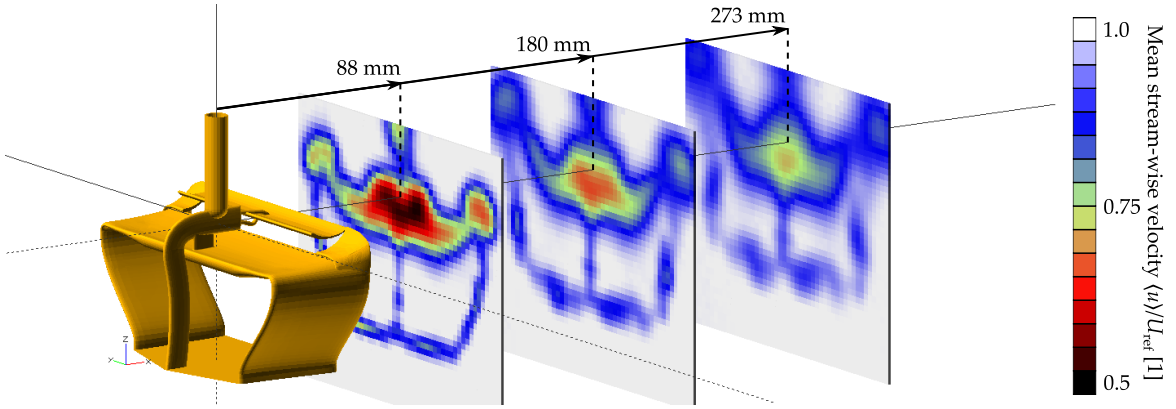

Figure 2. The sketch of measured planes in respect to the obstacle (model spoiler without a car) in open variant. The positions are measured from the axis of rod.

by using laser defocused in one direction to form the plane (or laser-sheet). The illuminated particles are observed by a pair of cameras from two directions. The combined images of a single scene allows to measure not only the motion on illuminated plane, but also in a direction perpendicular to it. Of-course, the *plane* has to have a finite thickness in order of millimeters, in order to the moving particle to still be illuminated in the following snapshot. The laser and the cameras operate in a double-pulse regime, the two pulses are separated by $\Delta T = 350\,\mu s$ (used in the current experiment for velocity $U_{ref} = 5\,m\,s^{-1}$). Details about the processing can be found in literature [20] and the uncertainty is discussed in article [21]. The images are processed using commercial software Dantec Dynamic Studio into a number of stereo vector fields. These vector fields are exported and further processed by home-made software [22].

3. Results

3.1. Mean field

Figures 3 and 4 display the measured mean velocity fields in three explored planes downstream of two variants of the spoiler wing. We can clearly observe that the open variant (left columns of Figures 3 and 4) keeps the wake core approximately at the same vertical (z) position, while the vortices past the wing bend move slightly upwards. Accordingly, past the closed variant, the entire wake core moves similarly as the vortices. This upward motion is associated with the force produced by this wing, as expected – the change of fluid's momentum is equal to the acting force [23]. The up-movement depicted in colour in Figure 4 is much stronger past the closed variant, however, it is partly compensated by the strong stream-wise vortices pushing the fluid down outwards of the wake. The stream-wise velocity deficit and thus expected drag force is much stronger in the closed variant as well, hence one can conclude that the change of the angle of attack of the central part of the spoiler wing affects the vehicle performance as expected, although the shorter edges of the wing, which are not changing

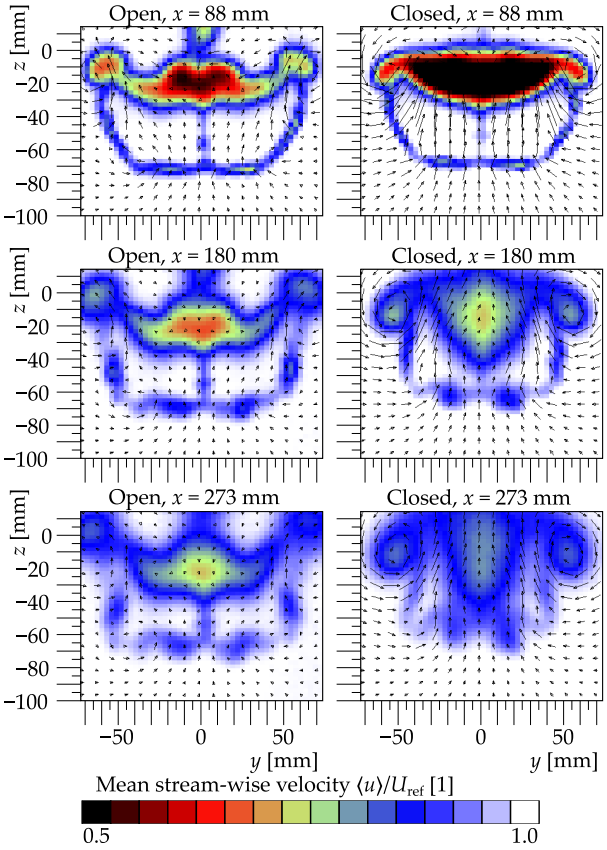

Figure 3. Spatial map of mean stream-wise velocity in three measured planes downstream the model. Left: *open* spoiler to decrease drag. Right: *closed* to increase negative lift.

the angle of attack, still produce a stream-wise vortex and a weak extra lift and drag.

3.2. Stream-wise vortices

The arrows in Figures 3 and 4 show the vortices in the mean field, especially past the closed variant of the wing. However, the spatial distribution of mean stream-wise vorticity $\langle \omega_x \rangle_T$ in Figure 5 is not so convincing, mainly past the open variant. The reason is that vorticity is sensitive not only to rotation but

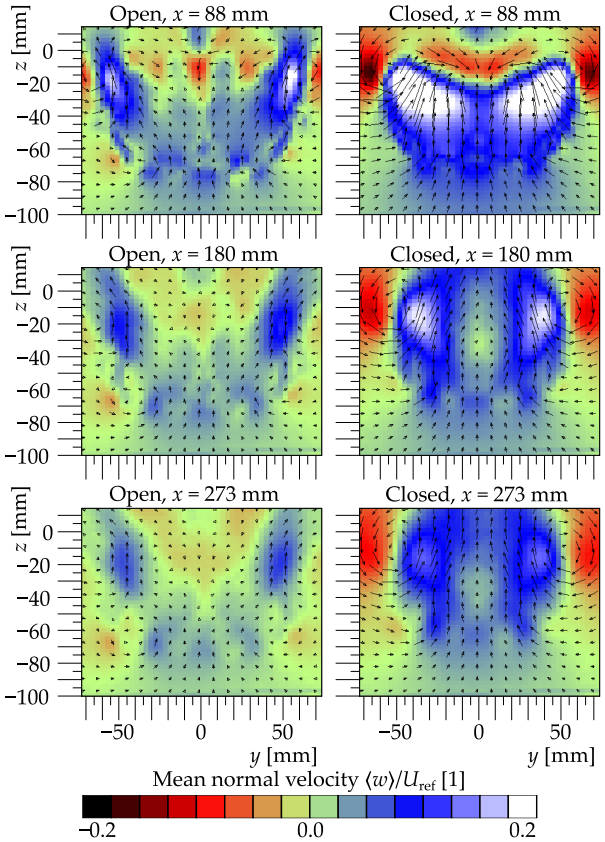

FIGURE 4. Spatial map of mean normal velocity in three measured planes downstream the model. Note that red colors correspond to downwards flow and thus contribute to *lift*, while the blue ones represent vertical movement of the air and thus contribute to negative lift (downforce).

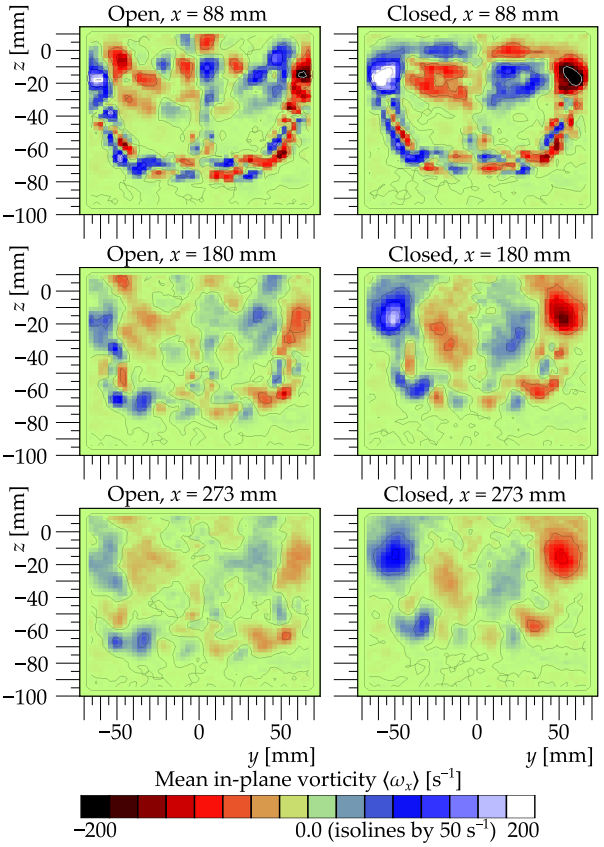

FIGURE 5. Mean stream-wise vorticity in inverse seconds.

to shear as well. To face this mathematical property, many of other parameters have been proposed [26–28], here we can look at the spatial distribution of Graftieaux's Γ_2 criterion [24] calculated as:

$$\Gamma_2(\vec{x};r) = \\ = \frac{1}{N}\sum_{\forall\vec{y},|\vec{x}-\vec{y}|\leq r} \frac{(\vec{x}-\vec{y})\times\left(\vec{u}(\vec{y})-\langle\vec{u}\rangle_{|\vec{x}-\vec{y}|\leq r}\right)}{|\vec{x}-\vec{y}|\cdot\left|u(\vec{y})-\langle\vec{u}\rangle_{|\vec{x}-\vec{y}|\leq r}\right|}. \quad (1)$$

This parameter *geometrically* quantifies the ratio of velocity vectors orbiting a certain point $\vec{x}$ within an area of radius r. This radius is an arbitrary parameter of this method and makes it a non universal solution, hence the λ_2 criterion [27] is used in the majority of works to detect vortices. In Equation (1), N is the number of velocity vectors in an area of radius r and $\langle u\rangle_{|\vec{x}-\vec{y}|\leq r}$ represents the average velocity in that area.

Figure 6 shows the spatial distribution of Γ_2 with chosen radius $r = 8.8\,\text{mm}$ at the middle position (distance $x = 180\,\text{mm}$) for the open and closed variants. In contrast to ω in Figure 5, here, the presence of strong stream-wise vortices even past the open variant is evident. The vortex is weaker (as expected), but its geometrical signature is strong enough. This observation allows us to apply the *individual vortex searching algorithm* [22, 25] with Oseen vortex model:

$$u_\theta(r) = \frac{\Gamma}{2\pi R}\cdot\frac{R}{r}\cdot\left(1-e^{-\left(r\cdot R^{-1}\right)^2}\right), \quad (2)$$

where r is the actual distance from the vortex centre, R is the vortex core radius and Γ is vortex core circulation, however, due to numerical stability, this is not a fitting parameter – the circumferential velocity in the form:

$$G = \frac{\Gamma}{2\pi R} \quad (3)$$

is used instead.

The vortices fitted to mean fields are shown in Figure 6b as colour circles for different distances past the obstacle. These mean-field vortices are used as an *ansatz* for instantaneous vortices in order to be sure that the correct vortex is selected (see the wilderness in Figure 6a) and that these vortices are indexed properly (i.e. the left vortex always has an index of 0 and the right one has an index of 1).

Figures 7 and 8 show the distribution of properties of fitted vortices: the core radii and circumferential velocities. Radii display wide distribution, which is wider and more flat in the case of the closed variant, past the open variant, the radii are more concentrated around smaller values. There is no strong observable stream-wise development.

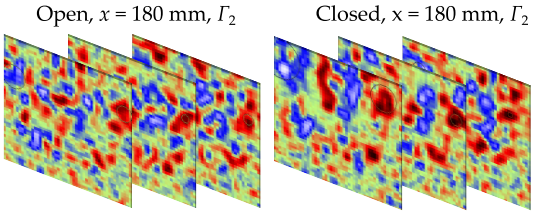

(a). Spatial distribution of Graftieaux's Γ_2 criterion [24] in few instantaneous snapshots in the distance of $x = 180$ mm.

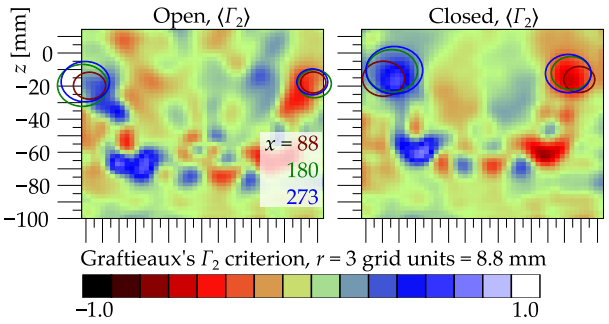

(b). Ensemble averaged Γ_2 (note that it si different from Γ_2 of mean field) and the color circles depict positions of vortices in mean field detected by using our method [22, 25].

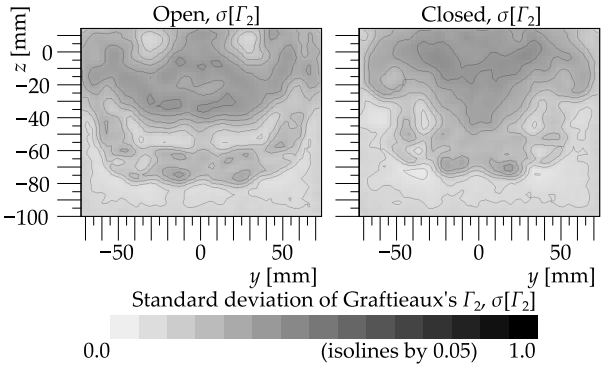

(c). Standard deviation of the ensemble.

Figure 6. Analysis by using Garftieux's Γ_2 criterion.

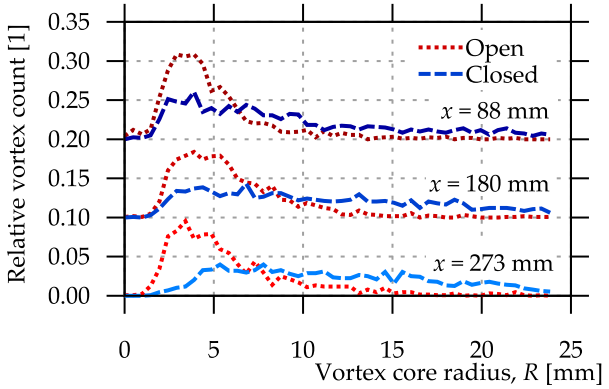

Figure 7. Histograms of vortex core radii of individual vortices.

The circumferential velocities behave as expected – larger values past the closed variant, and it decreases downstream. Due to non-linear damping, the outliers lose more energy and the distribution gets narrower

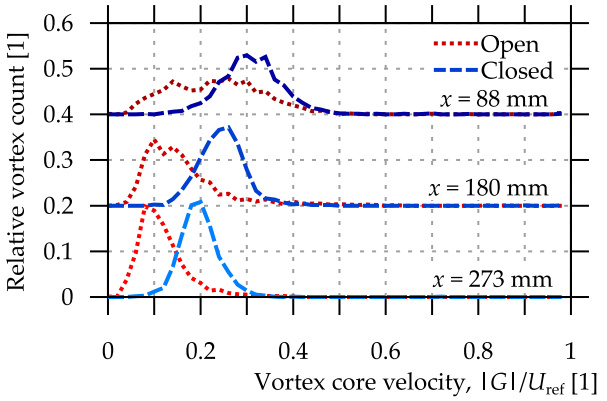

Figure 8. Histograms of circumferential velocities G of the individual vortices.

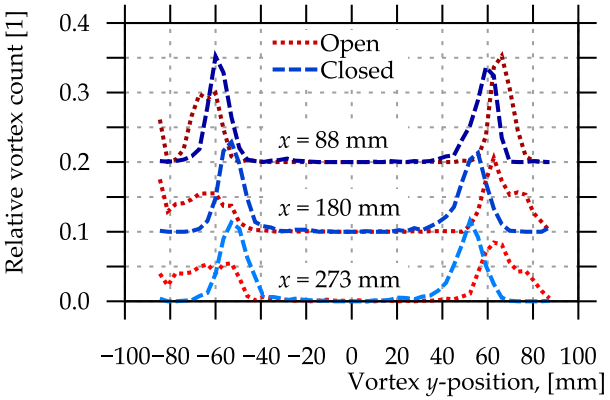

(a). y-coordinate (horizontal in figures).

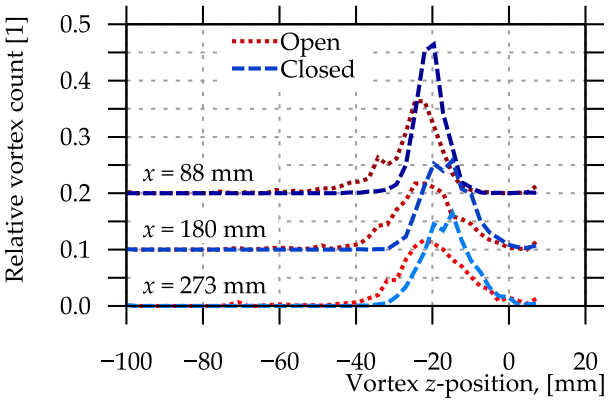

(b). z-coordinate (vertical in figures).

Figure 9. Histograms of the individual vortex positions.

with the distance, which is more observable past the open variant.

Two in-plane vortex positions (y and z) are another two fitting parameters (i.e. four in total). Their distribution is shown in Figure 9. The top panel shows the y-position (i.e. horizontal in other figures) and we can clearly see two maxima, which widen and are approaching each other as move downstream. For the closed variant, this approaching is more pronounced, while widening is more pronounced for the open variant. Additionally, some asymmetry caused by non-ideal

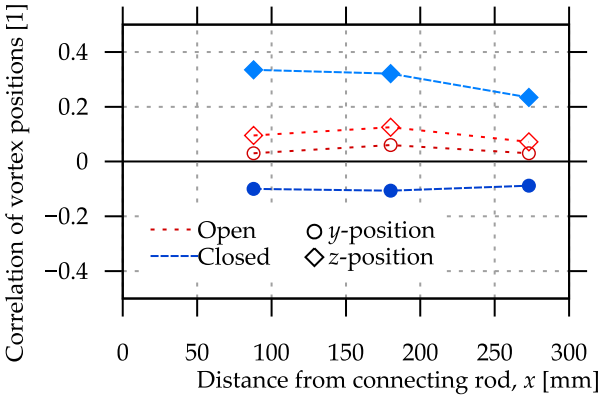

FIGURE 10. Stream-wise development of correlation between positions of detected vortices. Filled blue symbols and dashed lines represent closed variant, while the open red symbols and dotted lines play for open variant.

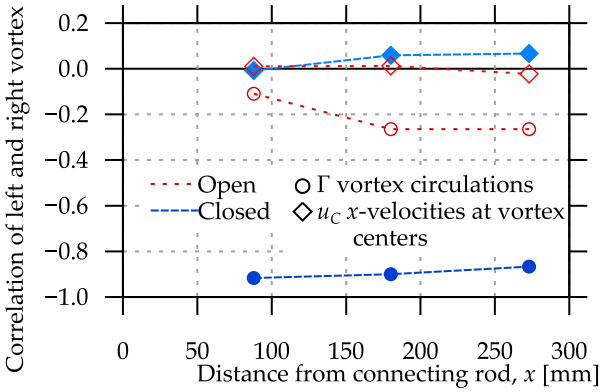

FIGURE 11. Correlation of left and right vortex circulations Γ (circles) and stream-wise velocities at vortex center u_C (diamonds).

mounting of the model inside the wind-tunnel can also be seen. Vertical positions (z) display upwards drifting and distribution widening as well.

3.3. Vortex correlations

Correlation of vortex parameters allows us to discover some coherent behaviour, if it exists. However, it is important to keep in mind that zero correlation does not mean independence (it can just mean a phase shift by $\frac{\pi}{2}$), and that existing correlation signify some causality, however, the *arrow* of causality cannot be determined by correlation only. The correlation R of vortex parameter y (or other) is calculated as follows:

$$R_{yy} = \frac{\langle (y_0 - \langle y_0 \rangle_T) \cdot (y_1 - \langle y_1 \rangle_T) \rangle_T}{\sigma_T[y_0] \cdot \sigma_T[y_1]}, \qquad (4)$$

where y_0 signifies y-coordinate of the left vortex, while y_1 that of the right one. $\langle y_i \rangle_T$ represents the ensemble average over measured snapshots of left/right vortices in each snapshot (time T). Similarly, $\sigma_T[y_i]$ is the standard deviation in respect to the ensemble.

The y-position shows a slight *anti*correlation (only about $\sim 10\,\%$, see Figure 10 (blue circles)) for the closed variant, which means that statistically, vortices move towards each other or oppositely. But the statistical coincidence is only $10\,\%$. In the case of the open variant, the correlation is positive, but it is so small, that it can be considered as statistically negligible. However, as mentioned above, it *can* signify a phase shift of some wave propagating on the vortex pair. Only a time-resolved PIV could answer this question.

Conversely, the correlation of z-positions (up-down) is positive and around $\sim 30\,\%$, suggesting that both vortices move together up or down. The open variant displays weaker signal again. In all cases, it weakens downstream.

Very interesting is the strong correlation of vortex circulations plotted in Figure 11 as circles. Note that vortices rotate oppositely, thus circulations have an opposite sign and negative correlation stays, that if the left one is faster, then the right one is faster as well but in the opposite direction. Again, the open variant displays a weaker correlation, under $30\,\%$. The correlation of vortex circulations weakens downstream past the closed spoiler, while that past the open variant is weakly correlated in the vicinity; the correlation establishes in larger distances.

One could argue, that this observed correlation might be connected, for example, to fluctuations of the wind tunnel velocity or the fluctuations of the entire wake. Such a hypothesis is disproven by the correlation of stream-wise velocities in the vortex centers, which display very small correlation past both variants as it is shown by using diamonds in Figure 11. Therefore, the correlation of circulations is a consequence of collective dynamics [5] of a vortex pair, not that of the wake.

4. Conclusion

An adjustable spoiler for cars of brand Škoda has been developed by prof. Zdeněk Hejda at the Škoda Auto University. The spoiler can switch between two configurations: *open* and *closed*. These two variants were 3D printed and measured in wind tunnel at the University of West Bohemia. Particle Image Velocimetry (PIV) has been used to map the velocity field in three planes behind the spoiler.

The closed variant displays a wider wake with deeper velocity deficit and stronger upwind. Surprisingly, the velocity deficit past the open variant sustains longer as the wake is more stable [29]. In both cases, strong wing-tip vortices are formed, although the spoiler does not have tips – the airfoil profile converts into thin sheet and turns down (see Figure 1). When closed, these vortices are stronger, as expected. They migrate towards each other. Their meandering displays weak anticorrelation ($\sim -10\,\%$) in horizontal plane and correlation ($\sim 30\,\%$) in vertical plane. Strong correlation of vortex strength suggest independent energy sources and interaction through the wake.

We feel that it is important to emphasise two major troubles connected with cars: the first one is the *safety*, the second one is the *ecology*. The *correct usage* of Hejda's spoiler could eliminate the need for braking and consecutive acceleration at curves together with decreased air drag (and thus decreased emissions from both: engine and brakes). Additionally, closing the spoiler could increase the total breaking force in emergency situations.

However, we are afraid that the net effect will be negative as the improved adjustable aerodynamics will lead to a false feeling of safety and thus to more dangerous behaviour of drivers. But the exact analysis of such effects belongs into some psychological study. In total, we do not believe this component would have a positive impact to the nature and the safety of traffic. Instead, we recommend wise usage of cars only for the purposes, when neither a train, bus, bicycle, nor walking would suffice for the transportation needs.

List of symbols

U_{ref} Reference velocity used in Wind Tunnel experiment $[\mathrm{m\,s^{-1}}]$

u Stream-wise velocity component (perpendicular to measured planes) $[\mathrm{m\,s^{-1}}]$

v Span-wise velocity component (left-right in measured planes) $[\mathrm{m\,s^{-1}}]$

w Normal velocity component (up-down in measured planes) $[\mathrm{m\,s^{-1}}]$

G Circumferential velocity of the vortex core; $G = \frac{\Gamma}{2\pi R}$, where Γ is the circulation and R the core radius $[\mathrm{m\,s^{-1}}]$

R Radius of vortex core [mm]

Γ Circulation of a vortex, $\Gamma = \oint \vec{u} \cdot \mathrm{d}\vec{\ell}$. $[\mathrm{mm^2\,s^{-1}}]$

Γ_2 Graftieaux's Γ_2 criterion, here, radius of 3 grid points, i.e. 8.8 mm; see more details in [24]. [1]

ω Vorticity, $\vec{\omega} = \nabla \times \vec{u}$; here, only its x-component is calculated using second-order central differentiation scheme. $[\mathrm{s^{-1}}]$

$\langle \ldots \rangle$ Ensemble average [...]

$\sigma[\ldots]$ Standard deviation [...]

IA Interrogation area – the size of a virtual square on the captured snapshot, where the correlation of particle's translation is calculated. Here 1 IA = 2.92 mm [mm]

Acknowledgements

We would like to acknowledge the support of project SGS-2022-023. We thank to the PhD Infra project from Jan Ámos Komenský operational programme (OP JAK) No. CZ.02.02.02/00/22_012/0005200 for modernizing of PIV measurement equipment.

References

[1] L. Chng, J. Alber, D. Ntouras, et al. On the combined use of Vortex Generators and Gurney Flaps for turbine airfoils. *Journal of Physics: Conference Series* **2265**(3):032040, 2022. https://doi.org/10.1088/1742-6596/2265/3/032040

[2] R. Bardera, E. Barroso, J. Carlos Matías. Wingtip vortices of a biomimetic micro air vehicle. In *Vortex dynamics – From physical to mathematical aspects*, chap. 9. IntechOpen, 2022. https://doi.org/10.5772/intechopen.102748

[3] M. Dghim, M. Ferchichi, H. Fellouah. On the effect of active flow control on the meandering of a wing-tip vortex. *Journal of Fluid Mechanics* **896**:A30, 2020. https://doi.org/10.1017/jfm.2020.343

[4] M. Dghim, K. Ben Miloud, M. Ferchichi, H. Fellouah. Meandering of a wing-tip vortex in a grid-generated turbulent flow. *Physics of Fluids* **33**(11):115131, 2021. https://doi.org/10.1063/5.0057083

[5] D. Duda, V. Yanovych. Interaction of stream-wise vortices generated by swirler grid. *Physics of Fluids* **36**(5):055148, 2024. https://doi.org/10.1063/5.0207124

[6] S. Inkinen, M. Hakkarainen, A.-C. Albertsson, A. Södergøard. From lactic acid to poly(lactic acid) (PLA): Characterization and analysis of PLA and its precursors. *Biomacromolecules* **12**(3):523–532, 2011. https://doi.org/10.1021/bm101302t

[7] GOM, mbH. GOM acceptance test – Process description, acceptance test according to the guideline VDI/VDE 2634 Part 3, 2014.

[8] J. Vagovský, I. Buranský, A. Görög. Evaluation of measuring capability of the optical 3D scanner. In *Procedia Engineering*, vol. 100, pp. 1198–1206. 2015. https://doi.org/10.1016/j.proeng.2015.01.484

[9] F. Li, D. Stoddart, I. Zwierzak. A performance test for a fringe projection scanner in various ambient light conditions. In *Procedia CIRP*, vol. 62, pp. 400–404. 2017. https://doi.org/10.1016/j.procir.2016.06.080

[10] R. Mendricky. Determination of measurement accuracy of optical 3D scanners. *MM Science Journal* (December):1565–1572, 2016. https://doi.org/10.17973/MMSJ.2016_12_2016183

[11] V. Yanovych, D. Duda, V. Horáček, V. Uruba. Research of a wind tunnel parameters by means of cross-section analysis of air flow profiles. *AIP Conference Proceedings* **2189**(1):020024, 2019. https://doi.org/10.1063/1.5138636

[12] C. Tropea, A. Yarin, J. F. Foss. *Springer handbook of experimental fluid mechanics*. Springer Berlin, Heidelberg, Germany, 2007. https://doi.org/10.1007/978-3-540-30299-5

[13] R. J. Adrian. Twenty years of particle image velocimetry. *Experiments in fluids* **39**(2):159–169, 2005. https://doi.org/10.1007/s00348-005-0991-7

[14] A. K. Prasad. Stereoscopic particle image velocimetry. *Experiments in fluids* **29**(2):103–116, 2000. https://doi.org/10.1007/s003480000143

[15] V. Koschatzky, P. D. Moore, J. Westerweel, et al. High speed PIV applied to aerodynamic noise investigation. *Experiments in fluids* **50**(4):863–876, 2011. https://doi.org/10.1007/s00348-010-0935-8

[16] D. Duda, T. Jelínek, P. Milčák, et al. Experimental investigation of the unsteady stator/rotor wake characteristics downstream of an axial air turbine. *International Journal of Turbomachinery, Propulsion and Power* **6**(3):22, 2021. https://doi.org/10.3390/ijtpp6030022

[17] L. Porreca, Y. I. Yun, A. I. Kalfas, et al. Investigation of 3D unsteady flows in a two stage shrouded axial turbine using stereoscopic PIV and FRAP: Part I – Interstage flow interactions. In *ASME Turbo Expo 2006: Power for Land, Sea, and Air*, vol. 6, pp. 711–723. 2006. https://doi.org/10.1115/GT2006-90752

[18] F. Scarano. *Particle Image Velocimetry*, chap. Overview of PIV in supersonic flows, pp. 445–463. Springer Berlin Heidelberg, 2007. https://doi.org/10.1007/978-3-540-73528-1_24

[19] J. Hong, M. Toloui, L. P. Chamorro, et al. Natural snowfall reveals large-scale flow structures in the wake of a 2.5-MW wind turbine. *Nature Communications* **5**(1):4216, 2014. https://doi.org/10.1038/ncomms5216

[20] M. Raffel, C. E. Willert, F. Scarano, et al. *Particle image velocimetry: A practical guide*. Springer, 2018. https://doi.org/10.1007/978-3-319-68852-7

[21] A. Sciacchitano, B. Wieneke. PIV uncertainty propagation. *Measurement Science and Technology* **27**(8):084006, 2016. https://doi.org/10.1088/0957-0233/27/8/084006

[22] D. Duda. Searching of individual vortices in experimental data. In I. Bakırtaş, N. Antar (eds.), *Vortex Dynamics – From Physical to Mathematical Aspects*. IntechOpen, 2021. https://doi.org/10.5772/intechopen.101491

[23] I. Newton. *Philosophiae Naturalis Principia Mathematica*, p. 83. Edmond Halley, 1687. [2025-07-03]. https://archive.org/details/newtonspmathema00newtrich/page/n87/mode/2up

[24] L. Graftieaux, M. Michard, N. Grosjean. Combining PIV, POD and vortex identification algorithms for the study of unsteady turbulent swirling flows. *Measurement Science and Technology* **12**(9):1422, 2001. https://doi.org/10.1088/0957-0233/12/9/307

[25] D. Duda. Individual vortex searching algorithm. In D. Šimurda, T. Bodnár (eds.), *In Proceedings Topical Problems of Fluid Mechanics 2020*, pp. 56–63. 2020. https://doi.org/10.14311/TPFM.2020.008

[26] G. Haller. An objective definition of a vortex. *Journal of Fluid Mechanics* **525**:1–26, 2005. https://doi.org/10.1017/S0022112004002526

[27] J. Jeong, F. Hussain. On the identification of a vortex. *Journal of Fluid Mechanics* **285**:69–94, 1995. https://doi.org/10.1017/S0022112095000462

[28] J. R. C. Hunt, A. A. Wray, P. Moin. Eddies, streams, and convergence zones in turbulent flows. *Proceedings of the Summer Program 1988* pp. 193–208, 1988.

[29] D. Duda, V. Uruba, V. Yanovych. Wake width: Discussion of several methods how to estimate it by using measured experimental data. *Energies* **14**(15):4712, 2021. https://doi.org/10.3390/en14154712